LUND UNIVERSITY

N=50 Core Excited States Studied in the 96Pd Nucleus

Palacz, M.; Nyberg, J.; Grawe, H.; Sieja, K.; de Angelis, G.; Bednarczyk, P.; Blazhev, A.; Curien, D.; Dombradi, Z.; Dorvaux, O.; Ekman, Jörgen; Galkowski, J.; Gorska, M.; Iwanicki, J.; Jaworski, G.; Kownacki, J.; Ljungvall, J.; Moszynski, M.; Nowacki, F.; Rudolph, Dirk; Sohler, D.; Wolski, D.; Zieblinski, M.

Link to publication

$N = 50$ core excited states studied in the $^{96}_{46}$Pd$_{50}$ nucleus

M. Palacz,[1] J. Nyberg,[2] H. Grawe,[3] K. Sieja,[4] G. de Angelis,[5] P. Bednarczyk,[6] A. Blazhev,[3,7,*] D. Curien,[4] Z. Dombradi,[8]
O. Dorvaux,[4] J. Ekman,[9] J. Gałkowski,[1,10] M. Górska,[3] J. Iwanicki,[1] G. Jaworski,[1,10] J. Kownacki,[1] J. Ljungvall,[11]
M. Moszyński,[12] F. Nowacki,[4] D. Rudolph,[9] D. Sohler,[8] D. Wolski,[12] and M. Ziębliński[6]

[1]*Heavy Ion Laboratory, University of Warsaw, ul. Pasteura 5A, 02-093 Warszawa, Poland*
[2]*Department of Physics and Astronomy, Uppsala University, S-75120 Uppsala, Sweden*
[3]*GSI Helmholtzzentrum für Schwerionenforschung, D-64291 Darmstadt, Germany*
[4]*Université de Strasbourg, IPHC, 23 rue du Loess 67037 Strasbourg, France, CNRS, UMR7178, 67037 Strasbourg, France*
[5]*INFN, Laboratori Nazionali di Legnaro, I-35020 Legnaro, Italy*
[6]*The H. Niewodniczański Institute of Nuclear Physics, Polish Academy of Sciences, 31-342 Kraków, Poland*
[7]*Faculty of Physics, University of Sofia, BG-1164 Sofia, Bulgaria*
[8]*Institute of Nuclear Research ATOMKI, Hungarian Academy of Sciences, H-4001 Debrecen, Hungary*
[9]*Department of Physics, University of Lund, S-22100 Lund, Sweden*
[10]*Faculty of Physics, Warsaw University of Technology, 00-661 Warszawa, Poland*
[11]*CSNSM, Bâtiments 104 et 108, 91405 Orsay Cedex, France*
[12]*National Centre for Nuclear Research, 05-400 Otwock-Świerk, Poland*

The four-proton hole ^{96}Pd neighbor of the doubly-magic ^{100}Sn nucleus was studied in-beam, using a fusion-evaporation reaction of a ^{58}Ni beam on a ^{45}Sc target. States of ^{96}Pd were established up to an excitation energy of 9707 keV. A core-excited odd-parity isomer with $T_{1/2} = 37.7(1.1)$ ns was identified. Shell model calculations were performed in four different model spaces. Even-parity states of ^{96}Pd are very well reproduced in large-scale shell model (LSSM) calculations in which excitations are allowed of up to five $g_{9/2}$ protons and neutrons across the $N = Z = 50$ gap, to the $g_{7/2}$, $d_{5/2}$, $d_{3/2}$, and $s_{1/2}$ orbitals. The odd-parity isomer can be only qualitatively interpreted though, employing calculation in the full fpg shell model space, with just one particle-hole core excitation.

I. INTRODUCTION

The region of the Segré chart around the heaviest self-conjugate doubly-magic nucleus ^{100}Sn has been, for decades, a subject of extensive experimental and theoretical investigations, providing a unique testing ground for the nuclear shell model. Studies in this region are stimulated by the existence of a variety of unresolved problems. First of all, nuclei approaching the $N = Z$ line are believed to be candidates for a new type of (deuteron-like) pairing, but different theories disagree on this matter [1–3]. Second, the energies of the single-particle levels in ^{101}Sn are widely debated due to two contradictory experimental claims [4,5]. Third, a new spin-aligned isoscalar ($T = 0$) proton-neutron coupling scheme has recently been proposed to be important in nuclei in the vicinity of ^{100}Sn [6]. The newly established low-lying excited states in ^{92}Pd were interpreted as a signature of the formation of four $T = 0$ proton-neutron pairs in this nucleus, each coupled to the maximum spin. It has also been shown that the isoscalar component of the proton-neutron interaction is essential for the formation of a high-spin isomer in ^{96}Cd [7]. However, the new coupling scheme still needs to be probed by large-scale shell model calculations, to confirm the dominance of the proposed $g_{9/2}$ aligned pairs in the realistic wave functions.

Finally, the rapid proton capture process path traverses the region, extending towards its anticipated end-point, which is located just above ^{100}Sn. Thus, knowledge of the structure of the involved nuclei and their neighbors is essential for the understanding of the abundance of the elements in the Universe [8]. In all these contexts, the underlying shell structure of nuclei in the vicinity of ^{100}Sn has to be determined with the highest possible accuracy.

The level structure at low excitation energy of nuclei located immediately below ^{100}Sn is rather well described in the basic shell model space with a rigid core at $N = Z = 50$ and valence holes or particles, which are located in the $g_{9/2}$, $p_{1/2}$ or $d_{5/2}$, $g_{7/2}$, $s_{1/2}$, and $d_{3/2}$ orbitals. It has, however, been recently demonstrated that the inclusion of the odd-parity $p_{3/2}$ and $f_{5/2}$ orbitals from below the $Z = 38$ gap, which opens up the entire fpg shell, is necessary for reproducing the decay properties of the observed spin-gap isomers in ^{94}Pd [9] and ^{96}Ag [10]. Moreover, one of the key points and questions in the region is the role of the excitations of the $N = Z = 50$ core. These were discussed already in the 1980s for $N = 50$ isotones [11]. States in $^{93}_{43}$Tc$_{50}$, $^{94}_{44}$Ru$_{50}$, and $^{95}_{45}$Rh$_{50}$ were described as single-neutron particle-hole excitations $\nu d_{5/2} g_{9/2}^{-1}$ coupled to the valence proton states of the fpg shell [12]. More recently, excitations of the $N = Z = 50$ core have been extensively studied in several closer $Z < 50$ neighbors of ^{100}Sn: ^{101}In [13], ^{102}In [14,15], ^{98}Cd [16,17], ^{99}Cd [13], ^{96}Ag [10], and ^{97}Ag [18]. The core excited states in these nuclei are in general successfully interpreted in the shell model space consisting of only even-

---

parity orbitals, with proton (and neutron) valence holes located in the $g_{9/2}$ orbital and particle-hole excitations across the $N = Z = 50$ gap to the $g_{7/2}$, $d_{5/2}$, $d_{3/2}$, and $s_{1/2}$ orbitals. A size of the $N = 50$ gap of about 6.5 MeV was inferred from such studies [10,16]. Odd-parity orbitals, for the description of such core excitations, have so far seemed unnecessary, as negative-parity core-excited states were not experimentally observed in any of the above-mentioned close neighbors of ^{100}Sn.

In the present work we analyze excited states of the nucleus $^{96}_{46}$Pd$_{50}$, which has four valence proton holes outside ^{100}Sn. We establish a rather rich sequence of states in this nucleus up to an excitation energy of 9707 keV and a tentative spin and parity of 19^+. Most of the newly observed states are interpreted as $N = 50$ core excitations. Among those, a negative-parity isomeric state is identified.

The ^{96}Pd nucleus was previously studied both in β decay [19,20] and in-beam [21–23]. Excited yrast states were earlier established up to the 12^+ state at 4573 keV, which is the highest spin that can be created with four proton holes in the $g_{9/2}$ and $p_{1/2}$ orbitals. Above this state, two additional excited states were identified at excitation energies of 6728 and 7039 keV. These states were interpreted as $N = 50$ core excitations. The spin of the 6728 keV level could only be tentatively proposed based on the analogy to the core excitation of ^{94}Ru and using shell model arguments. A long-lived 8^+ seniority isomer with a half-life of 2.2(3) μs was identified at an excitation energy of 2530 keV (see also Ref. [24]). A half-life of 7.5(10) ns was as well measured for the 6^+ state. Another delayed component was seen in the time distributions of the transitions above the 8^+ isomer, with a half-life of $T_{1/2} = 35(4)$ ns, and it was associated with a level at 7039 keV, leading also to the 15^+ tentative spin assignment for this state. G factors of 1.37(1) [21] and 0.83(5) [23] were measured for the 8^+ state and for the high-spin isomer, respectively. In addition, a state was observed at an excitation energy of 2649 keV [20,23] and it was interpreted as a 5^- state, with one proton hole in the $p_{1/2}$ orbital. The β-decay work of Ref. [20] established also a few other non-yrast positive-parity excited states.

II. EXPERIMENT AND DATA EVALUATION

Excited yrast states in very neutron-deficient nuclei in the vicinity of ^{100}Sn can be populated and studied by using stable beams either in heavy-ion induced fusion-evaporation reactions or in fragmentation experiments. The latter possibility is restricted so far to states below isomers with half-lives in the μs range, down to hundreds of ns. In any case, the nuclei of interest are produced with very small cross sections. Sophisticated setups of detectors must, thus, be used in order to select the required reaction products.

In this work we present results of a fusion-evaporation experiment, which was performed at the Institut de Recherches Subatomiques in Strasbourg, France. A DC beam of ^{58}Ni ions with an energy of 205 MeV and an average intensity of 10 p nA was used to bombard a ^{45}Sc target, leading to the compound nucleus ^{103}In. Four ^{45}Sc targets with the thickness in the range from 9.7 to 10.6 mg/cm^2 were used consecutively during the experiment. The ^{45}Sc foil used for the production of targets

was 99.99% pure, but some oxygen contamination could be introduced to the target in the rolling process in air. A small accumulation on the targets of ^{16}O and ^{12}C was also observed during the experiment. The targets were thick enough to stop the recoiling nuclei produced in the reactions, as well as all the beam particles (which was the requirement imposed by the charged-particle detector).

Two neutrons, one α particle and one proton were emitted from the ^{103}In compound nucleus in events in which ^{96}Pd was populated. The EUROBALL γ-ray spectrometer [25,26] was used in a configuration consisting of 26 clover [27] and 15 cluster [28] high-purity germanium γ-ray detectors. In addition, the Neutron Wall consisting of 50 liquid scintillator detectors [29,30], and the plastic scintillator charged particle veto detector CUP [31] were employed for selection of events leading to very neutron-deficient nuclei. Information from the CUP detector was, however, not used in the part of the data analysis, that led to the observation of transitions from ^{96}Pd.

The experiment was run with two different trigger conditions applied for different periods of data taking. One γ ray in the Ge detectors was initially required together with one neutron in the Neutron Wall, while later during the experiment the required neutron fold was increased to two. This resulted in collecting about 5.7×10^8 and 2.2×10^9 events, with the one- and two-neutron conditions, respectively, with the total effective data-taking time of 14 days. At the hardware (trigger) level, neutrons and γ rays detected in the Neutron Wall were distinguished by using the zero-crossover method [29]. Note that in the following offline analysis the time of flight of neutrons between the target and detectors was also used to improve discrimination of neutrons and γ rays detected in the Neutron Wall (see below).

In the offline analysis the entire data set was scanned in intervals corresponding to about two hours of beam time each, and all the experimental parameters were semiautomatically checked and corrected by using the program ALIGN [32] for instrumental drifts and instabilities. The instabilities detected in the γ-ray energy spectra were corrected by applying linear corrections, while the time parameters where eventually modified using simple shifts (without changing the gain). No instabilities could be detected in the structureless energy spectra from the Neutron Wall detectors. The energy calibration and relative efficiency of the Ge detectors were determined using the standard radioactive sources ^{56}Co, ^{133}Ba, and ^{152}Eu.

A large effort was devoted to optimize the conditions to identify two neutrons detected in the Neutron Wall. First, the discrimination of neutrons and γ rays was improved by setting two-dimensional gates on the time of flight between the target and the detector vs the zero-crossover parameter. Second, events with two neutrons detected had to be distinguished from events in which a single neutron scattered in more than one detector. This was done by setting gates on the time difference between two interactions and the distance between the involved detectors. See Ref. [30] for more information on the Neutron Wall data evaluation and in particular on the $1n/2n$ discrimination.

The Neutron Wall detectors provided also the time reference for all other parameters. Such a time reference should preferably be given by a prompt γ ray detected in one of
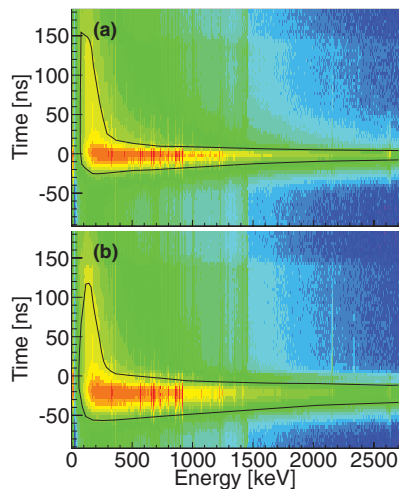
FIG. 1. (Color online) Gamma-ray energy vs time distributions seen in Ge detectors, for the two types of time references obtained from the Neutron Wall: (a) γ ray and (b) neutron. The two-dimensional gates, which were used to select prompt γ rays, are marked in the plots. The zero value on the time axis in both plots is set at the maximum of the distribution obtained with the γ-ray time reference.

FIG. 2. (Color online) Gamma-ray spectra obtained in the ^{58}Ni + ^{45}Sc reaction. The spectra shown in (a)–(c) are prompt and gated by (a) two neutrons, (b) two neutrons and the 790 keV γ-ray line, and (c) one neutron and the 2154 keV γ-ray line. Plot (d) is the same as (c), except that γ rays are not prompt, but delayed in the time range from 10 to 45 ns. The gamma-ray transition at 685 keV marked in plot (d) directly depopulates the isomer at 8384 keV, and the delayed contribution enhances also the 324 and 662 keV transitions, originating from the state at 7699 keV (see Fig. 3).

the Neutron Wall detectors. However, in a significant fraction of events (55% in case of events in which ^{96}Pd was produced) no γ rays were detected in the Neutron Wall. In such a situation the time reference was given by the fastest detected neutron, which was registered by the neutron detectors on average about 20 ns later than the prompt γ rays. This resulted in a delayed and broader time reference, compared to the one given by prompt γ rays. Note that the relative number events without a γ ray in the Neutron Wall strongly depends on the reaction channel, and varies between about 30% and 70%.

The time signals of the Ge detectors were calibrated by adding a 32 ns delay to the time reference signal, which was used as a common stop of the Ge time-to-amplitude converters. For the prompt evaluation of the γ-ray spectra, two energy-dependent time gates were set on the Ge detector signals, one for each type of the time references mentioned above; see Fig. 1. Double and triple prompt γ-ray coincidences were analyzed with such time conditions, for events with two neutrons detected. The numbers of double and triple coincidences were 1.1×10^8 and 2.7×10^7, respectively. Significant fractions of those coincidences were obtained as a result of unfolding higher γ-ray fold events.

In the work of Ref. [23], a γ-ray observation time limit from 10 to 45 ns was found to be favorable to enhance transitions depopulating the high-spin isomer in ^{96}Pd. Thus, $\gamma\gamma$-coincidence matrices with the same time condition were also created, with the requirements of registering at least one or two neutrons. The numbers of such coincidences were 1.1×10^7 and 6.6×10^5 for the 1n and 2n conditions, respectively. Time distributions of germanium detectors signals corresponding to selected γ-ray energies were also analyzed in order to determine half-lives of the isomeric state—see Sec. III.

Only limited information on the angular distribution properties of the γ rays could be obtained from the data. The angular
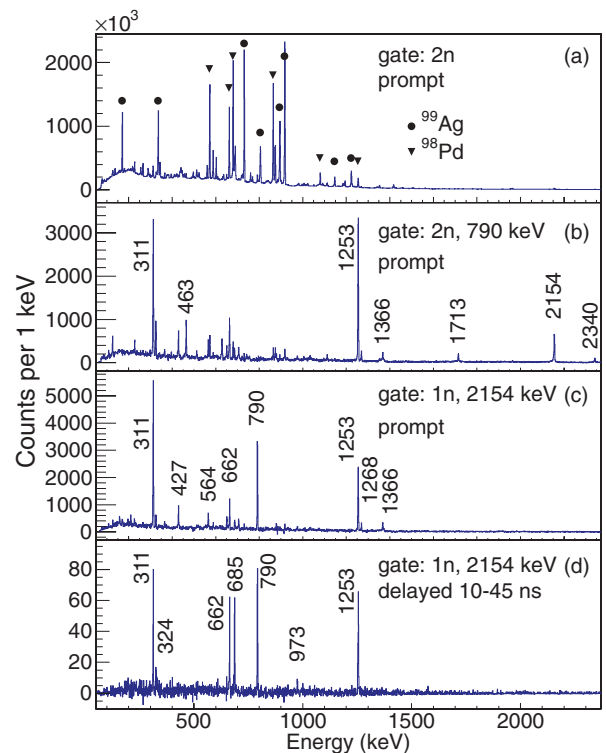
distribution ratios $R = I_{\theta_1}/I_{\theta_2}$ of γ-ray intensities measured at two different groups of angles with respect to the beam axis were determined. I_{θ_1} corresponds to the intensity measured in the cluster detectors at angles 123° and 164° and I_{θ_2} to the intensity in the clover detectors at 72° and 107°. This was done in spectra gated by a coincident γ ray observed at any direction, in order to obtain sufficiently clean peaks. Based on values obtained for transitions of known multipolarity, we expect approximately $R = 0.5$ and $R = 1.0$ for stretched dipole and quadrupole transitions, respectively, emitted from highly aligned states. Determining the R values allowed us to make tentative spin assignments for most of the observed states, assuming that maximum spin states are preferably populated in a heavy-ion induced reaction, and that we do not observe prompt transitions of higher multipolarities than 2.

The RADWARE [33], ROOT [34] and TSCAN [35] software packages were used in the data evaluation.

III. RESULTS

Figure 2(a) shows a prompt γ-ray spectrum created with the condition that at least two neutrons were detected. With this condition, γ-ray transitions emitted from excited states in

12 different nuclei produced in the fusion-evaporation reaction of ^{58}Ni on ^{45}Sc could be identified. The most intense γ-ray transitions belong to ^{99}Ag (emission of two protons and two neutrons, $2p2n$) and ^{98}Pd ($3p2n$). The estimated production cross sections of ^{96}Pd, ^{99}Ag, and ^{98}Pd are 0.8, 11, and 6.2 mb, respectively. The cross-section values were obtained from the relative intensity of ground-state feeding transitions in one- and two-neutron gated γ-ray spectra. The measured yields were normalized to the sum of the cross sections of all the identified products of the reaction, calculated with the EVAPOR code [36] (237 mb), which in EVAPOR calculations corresponds to 80% of the total fusion-evaporation cross section.

Due to an imperfect discrimination of scattered neutrons, gamma-ray transitions from ^{99}Pd ($3p1n$) and ^{96}Rh ($2p1\alpha1n$) could be identified in the two-neutron gated spectra. In addition, due to imperfect neutron-gamma discrimination, a weak contribution from the strongest reaction channel with no neutrons emitted, ^{100}Pd ($3p$), could as well be identified in the two-neutron gated spectra. The probability that a γ ray emitted from the $0n$ and $1n$ reaction channels is erroneously accepted by the two-neutron condition can be estimated as $P_{xn\to2n} = I_{2n}/I_{\mathrm{tot}}$ ($x = 0, 1$), where I_{2n} and I_{tot} are intensities of this γ ray with the two-neutron condition and without any condition on detected neutrons, respectively. We obtain $P_{0n\to2n} = 3 \times 10^{-5}$ and $P_{1n\to2n} = 4 \times 10^{-4}$. Gamma-ray transitions from two nuclei produced in the reaction of the beam with the ^{12}C or ^{16}O target contaminants, namely ^{68}Se and ^{68}As, could also be identified in the two-neutron gated data.

The level scheme of ^{96}Pd constructed in this study is presented in Fig. 3(a). The information about the observed γ-ray transitions is summarized in Table I and examples of prompt γ-ray coincidence spectra gated on ^{96}Pd transitions are presented in Figs. 2(b) and 2(c).

We confirm the placements of all the previously observed [23] transitions, up to the level at 7037 keV, and we have identified 12 new excited states. The placement of most of the levels shown in Fig. 3 is firmly established by coincidence relationships and by the intensities of γ rays measured in the gated spectra, analyzed with double and triple γ-ray coincidences.

The measured angular distribution ratio R of the 2154 keV transition favors a spin difference of $\Delta J = 1$ between the connected states. Thus, we assign spin and parity (13^+) to the 6726 keV state, which supports the previous assignment based on systematics [23]. The R value for the 311 keV transition depopulating the 7037 keV state excludes a stretched quadrupole character of this transition, which gives $J^\pi = (14^+)$ for the 7037 keV state. In the work of Ref. [23] a spin value of $15\hbar$ was proposed for this state. This was based on the assumption that the 7037 keV state had a half-life of 35 ns and that it presumably decayed by a stretched $E2$ transition. This disagrees with our present results—see below.

The ΔI spin differences of the sequence of levels above the 7037 keV state, namely the states 7699, 8403, 8967, and 9280 keV, are supported by the presence of the crossover transitions (973, 1366, 1268, and 877 keV) of presumably stretched $E2$ character. This is corroborated by the low R values obtained for the 704 and 564 keV transitions. The (15^+) assignment of the 7699 state is also supported by the presence
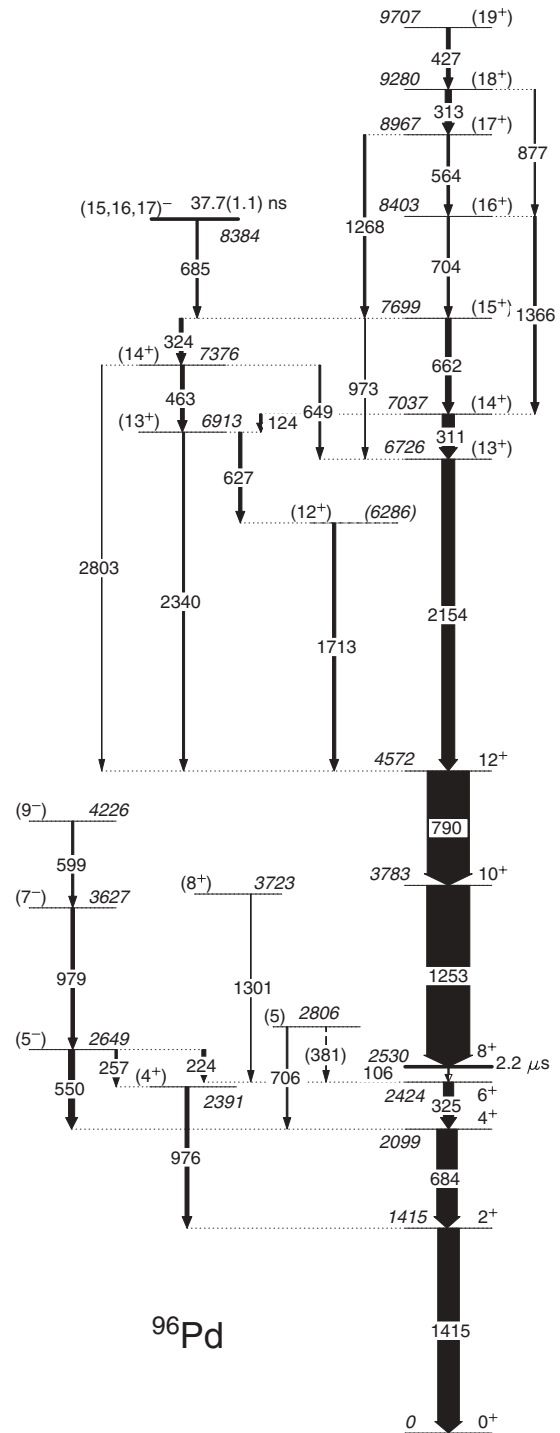
FIG. 3. Level scheme of ^{96}Pd established in this work. Widths of the arrows are proportional to the intensity of transitions seen with the prompt conditions of Fig. 1.

and angular distribution properties of transitions linking the yrare states 7376, 6913, and 6286 keV. The order of the 627 and 1713 keV transitions, linking the states at 6913 and 4572 keV, cannot be firmly established. Thus, the excitation energy of the (12_2^+) state at 6286 keV is treated as tentative. The 427 keV transition placed at the top of the level scheme has

TABLE I. Gamma-ray transitions assigned to ^{96}Pd. The following quantities are listed: γ-ray energy (E_γ), relative γ-ray intensity seen with the prompt conditions of Fig. 1 (I_γ), excitation energy of the initial state (E_i), angular distribution ratio (R), and the spin and parity assignments of the initial (J_i^π) and the final (J_f^π) state. Indexes in the R column indicate gating transitions used to determine R: (a) 790 keV, (b) 1253 keV, (c) 1415 keV, and (d) 550 keV.

E_γ (keV)	I_γ	E_i (keV)	R		J_i^π	$\rightarrow$	J_f^π
106.2(3)	1.43(20)	2530			8^+	$\rightarrow$	6^+
124.2(3)	4.7(5)	7037			(14^+)	$\rightarrow$	(13^+)
224.5(3)	9.2(10)	2649	0.67(6)	(c)	(5^-)	$\rightarrow$	6^+
257.2(3)	5.4(6)	2649			(5^-)	$\rightarrow$	(4^+)
311.0(3)	28(3)	7037	0.50(1)	(a,b)	(14^+)	$\rightarrow$	(13^+)
312.8(3)	14.2(15)	9280			(18^+)	$\rightarrow$	(17^+)
323.6(3)	8.8(9)	7699	0.46(5)	(a,b)	(15^+)	$\rightarrow$	(14^+)
325.2(3)	23.3(24)	2424	0.76(4)	(c)	6^+	$\rightarrow$	4^+
381.1(4)	1.5(3)	2806			(5^+)	$\rightarrow$	6^+
427.5(3)	8.8(9)	9707	0.48(3)	(a,b)	(19^+)	$\rightarrow$	(18^+)
462.8(3)	8.8(9)	7376	0.45(2)	(a,b)	(14^+)	$\rightarrow$	(13^+)
549.7(3)	14.2(15)	2649	0.45(4)	(c)	(5^-)	$\rightarrow$	4^+
564.0(3)	6.0(7)	8967	0.57(4)	(a,b)	(17^+)	$\rightarrow$	(16^+)
598.8(3)	5.0(6)	4226	0.84(7)	(c,d)	(9^-)	$\rightarrow$	(7^-)
627.2(3)	7.5(8)	6913	0.42(3)	(a,b)	(13^+)	$\rightarrow$	(12^+)
649.4(3)	4.2(5)	7376	0.7(1)	(a)	(14^+)	$\rightarrow$	(13^+)
662.1(3)	13.2(14)	7699	0.88(5)	(a,b)	(15^+)	$\rightarrow$	(14^+)
683.8(3)	47(5)	2099	0.75(3)	(c)	4^+	$\rightarrow$	2^+
685.2(3)	5.1(7)	8384				$\rightarrow$	(15^+)
703.7(3)	5.2(6)	8403	0.40(4)	(a,b)	(16^+)	$\rightarrow$	(15^+)
706.2(3)	3.7(5)	2806	0.54(10)	(c)	(5^+)	$\rightarrow$	4^+
789.8(3)	98(10)	4572	0.95(2)	(b)	12^+	$\rightarrow$	10^+
876.9(3)	3.1(4)	9280			(18^+)	$\rightarrow$	(16^+)
973.0(4)	1.21(24)	7699			(15^+)	$\rightarrow$	(13^+)
976.1(3)	9.1(12)	2391	0.66(8)	(c)	(4^+)	$\rightarrow$	2^+
978.9(3)	8.1(9)	3627	0.81(9)	(c,d)	(7^-)	$\rightarrow$	(5^-)
1252.9(3)	100(5)	3783	0.95(3)	(a)	10^+	$\rightarrow$	
1267.6(3)	5.7(6)	8967	0.88(7)	(a,b)	(17^+)	$\rightarrow$	(15^+)
1300.6(4)	1.5(3)	3723			(8^+)	$\rightarrow$	6^+
1365.6(3)	5.9(7)	8403	0.84(6)	(a,b)	(16^+)	$\rightarrow$	(14^+)
1415.2(3)	50.2(20)	1415			2^+	$\rightarrow$	0^+
1713.4(3)	7.5(9)	6286	0.69(5)	(a,b)	(12^+)	$\rightarrow$	12^+
2153.7(3)	30(3)	6726	0.71(3)	(b)	(13^+)	$\rightarrow$	12^+
2340.4(3)	4.8(5)	6913	0.36(3)	(a,b)	(13^+)	$\rightarrow$	12^+
2803.4(5)	0.85(18)	7376			(14^+)	$\rightarrow$	12^+

a low R value. Therefore, we assign $J^\pi = 19^+$ to the highest observed state at an excitation energy of 9707 keV.

All the transitions shown in the level scheme of Fig. 3, except the 685 keV transition depopulating the 8384 keV state (see below), were identified with the narrow time gates shown in Fig. 1. A delayed component was, however, clearly seen in the time distributions of the 1253, 790, and 2154 keV transitions, as reported in the earlier experiments [22,23]. A similar delayed component was also seen in the time distributions of the new 2340 and 1713 keV transitions— see Fig. 4 for the examples of time spectra. Fits of single exponential decay curves of time distributions in the range of approximately 37 to 137 ns relative to the prompt position gave for these five transitions a weighted average of the half-life of 37.7(1.1) ns. Prompt background was estimated using prompt transitions of similar energy and was subtracted from the spectra prior to the fits. We note that for the time analysis of the

2154, 2340, and 1713 keV transitions, a requirement of only one detected neutron was sufficiently selective, which could be checked in the corresponding $\gamma\gamma$-coincidence spectra, and which gave a significant gain in the statistics, compared to using the two-neutron gated spectra.

In the work of Ref. [23] the observed high-spin delayed component was tentatively associated with the decay of the 7037 keV excited state. This assignment is now excluded, by the presence of the delayed component in the time distributions of the 1713 and 2340 keV transitions. Note that the 124 keV transition feeding the 6913 keV state is too weak to account for the delayed component in the 2340 and 1713 keV transitions, in case the isomer were located at 7037 keV.

The search for a new placement of the high-spin isomeric state was, however, difficult because of many overlapping transitions. The time distributions of the 311 and 662 keV transitions were not informative: they are doublets with strong
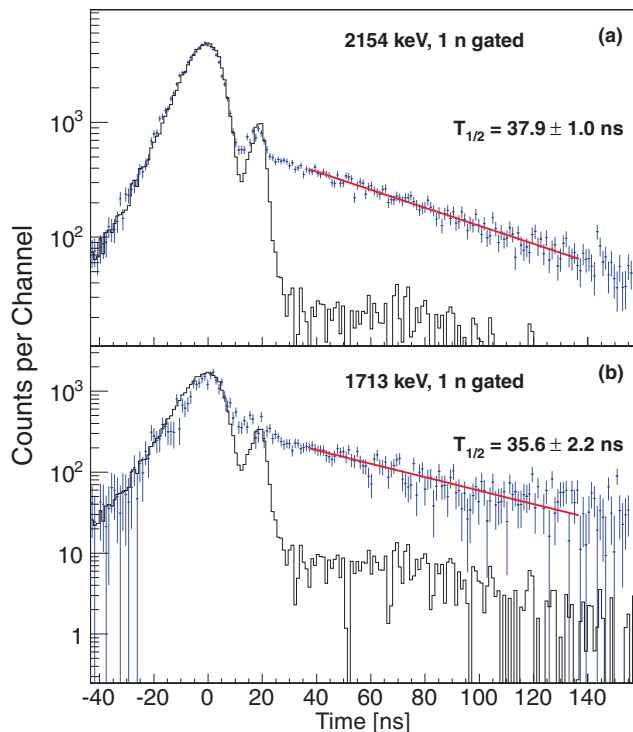
FIG. 4. (Color online) The data points show the time distributions of the (a) 2154 keV and (b) 1713 keV γ-ray transitions, measured with the neutron time reference. The zero value on the time axis is set at the prompt position. Fits of a single exponential decay curve to the time distributions in the range of approximately 37 to 137 ns are shown as solid lines and the resulting half-life values are given in the legend. Prompt background was subtracted from the spectra prior to the fits. A histogram of a prompt γ-ray with similar energy (2632 keV transition in ^{99}Ag) is drawn with solid lines. Peaks in the distributions at about 20 ns are due to residual contributions of events with the γ-ray time reference.

transitions in ^{98}Pd. The 324 keV transition, depopulating the 7699 keV level, is a doublet with the 325 keV transition, which is located below the 8^+ isomer ($T_{1/2} = 2.2\ \mu$s). The 463 keV transition is strongly contaminated by a transition of similar energy in ^{100}Cd. The 627 keV transition is too weak for the time distribution analysis if the $2n$ condition is used, and it is too much contaminated by a transition in ^{96}Rh if only the $1n$ condition is used. Similarly, the presence of a delayed component could not be directly verified for the other high-lying transitions, as they are either too weak or too much contaminated, or both.

In a further attempt to find a new placement of the isomeric state, the previously used [23] delayed-time condition, from 10 to 45 ns, was set on coincident γ rays. A γ-ray spectrum created with this time condition and gated on one neutron and the 2154 keV transition is presented in Fig. 2(d), while a prompt spectrum obtained with the same γ ray and neutron gates is shown in Fig. 2(c). In the delayed spectrum, all the yrast transitions placed in the level scheme below the 7699 keV state are seen; so are the 324 and 649 keV transitions linking the (14_2^+) state at 7376 keV. However, the transitions depopulating levels above 7699 keV are not visible. Instead, a new strong

685 keV transition is present. A comparison of these two spectra and the established prompt level scheme leads to the conclusion that a delayed 685 keV transition directly feeds the 7699 keV state, and thus the observed half-life should be associated with the new state at 8384 keV.

The fact that a transition of a very similar energy (684 keV) is depopulating the 6^+ level, situated below the 2.2 μs isomer, explains why the 685 keV delayed transition could not be identified in earlier studies, nor in our analysis of the prompt data. In the delayed spectrum of Fig. 2(d), the 1415 keV ground-state transition can not be seen at all, and this proves that the new 685 keV transition is different than the 684 keV $4^+ \to 2^+$ transition. We note that a strong transition with similar energy (688 keV) exists also in ^{99}Ag ($2p2n$ reaction channel in this experiment), which makes the direct analysis of the 685 keV transition in ^{96}Pd even more problematic.

Note that the delayed component of the γ-ray time distributions could only be identified in spectra created by using events with a time reference given by a neutron detected in the Neutron Wall (see Fig. 4). The delayed component is strongly suppressed in the corresponding spectra obtained by using the γ-ray time reference. The reason for this is that the requirement of registering a prompt γ ray in the Neutron Wall is hardly ever fulfilled in events in which a high-spin isomer is populated.

Our experimental data does not allow for a direct determination of the spin and parity of the 8384 keV state. Only states lying close to the yrast line should be populated in a heavy-ion induced reaction, which makes spin assignments outside the range from $15\hbar$ to $17\hbar$ very unlikely. In addition, the observed rather regular sequence of $\Delta I = 1$ positive parity states above the 12_1^+ state leaves no space for a positive-parity yrast or yrare isomer, which should decay via an $E2$ transition. Note that a similar prompt sequence above 12^+ is seen in the next lighter $N = 50$ isotone $^{94}_{44}$Ru$_{50}$ [12] (Fig. 5), and fast M1 transitions are in fact expected between core excited states with similar and large magnetic moments. In particular, a $J^\pi = 17^+$ assignment to the isomer would make the higher-lying states highly non-yrast. Any lower spin value and positive parity requires exceptionally strong and unlikely hindrance of $M1$ and $E2$ decay modes to lower states, in order to make the delayed 685 keV transition favorable. If the decay mode is $E2$, such a hindrance should in addition overcome the E^5 factor for 1 MeV or higher energy transitions to 14^+ or possibly lower spin states.

The odd-parity states in ^{94}Ru exhibit a regular $\Delta J = 1$ sequence too, but the states with even spins show a trend of approaching the higher odd spins—see the $14^- - 15^-$ and $16^- - 17^-$ pairs, and compare also to states in $^{92}_{42}$Mo$_{50}$ (Ref. [37] and Fig. 5). A $J = 2n$ to $J + 1$ order may, thus, eventually be inverted in ^{96}Pd to make the even-spin states non-yrast. This would disable $M1$ decays of the natural-parity odd-spin states and enable $E1$ modes to positive-parity states or $E2$ transitions within the negative-parity cascade. Thus, we conclude that the possible spin and parity assignment for the 8384 keV state is $J^\pi = (15, 16, 17)^-$.

A possibility should also be evaluated that the isomeric state in fact lies slightly above 8384 keV, and feeds the 8384 keV state via a low-energy unobserved transition. We
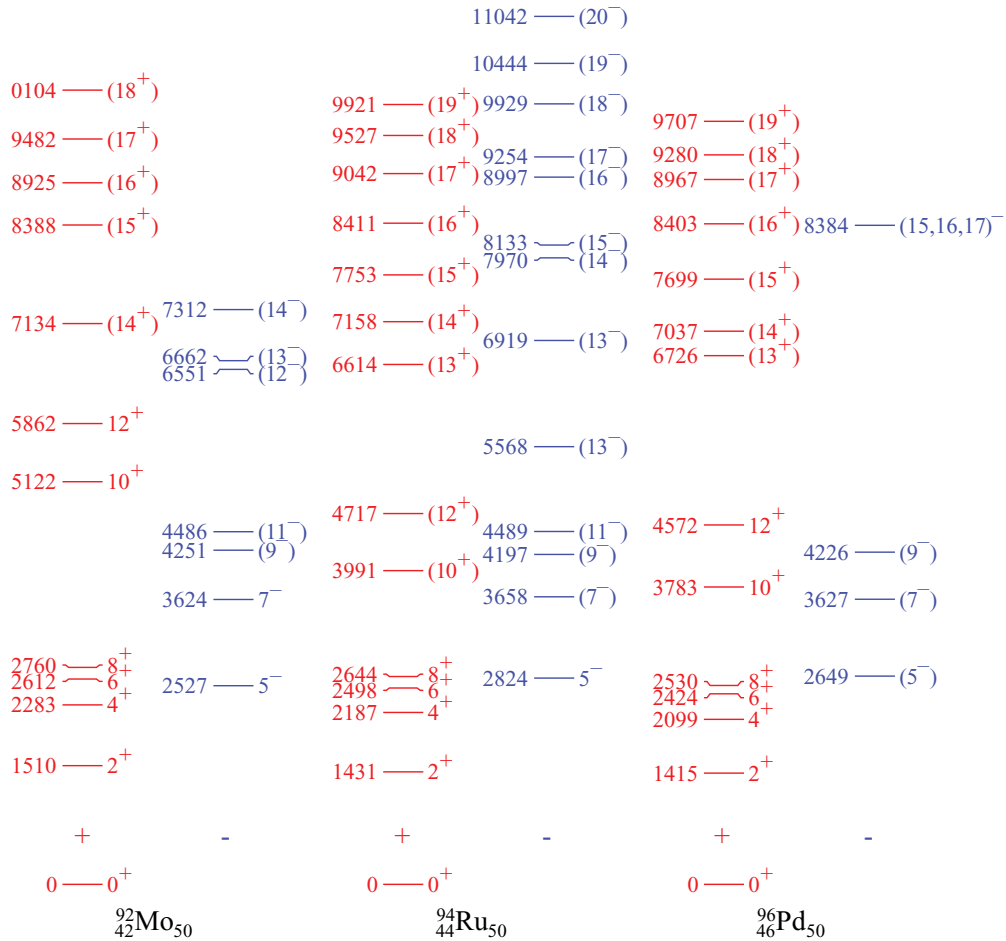
FIG. 5. (Color online) Even and odd-parity experimental yrast states in the $N = 50$ isotones ^{92}Mo [37], ^{94}Ru [12], and ^{96}Pd. For ^{94}Ru two 13^- states are plotted: one corresponding to the pure $p_{1/2}^{-1}g_{9/2}^{-5}$ configuration, which uniquely exists in ^{94}Ru, and another one due to the core excitation, at 5568 and 6919 keV, respectively.

estimate that the experimental upper energy limit for such an unobserved $E2$ transition is about 100 keV, taking into account the internal conversion coefficients, the efficiency of the setup, and statistics with the necessary gating conditions. For an unobserved $E1$ transition, the energy limit is slightly lower. The possible existence of an unobserved low-energy transition leaves in place the spin and parity restrictions discussed above. In fact, an additional transition makes the yrast conditions even more difficult to fulfill. Out of several sequences of the isomer decay to the 15^+ state at 7699 keV which could be listed, we consider only the $17^- \rightarrow 16^+ \rightarrow 15^+$ path possible and in agreement with the $N = 50$ systematics.

In addition to the states at high excitation energy discussed above, a few new states with lower spins and excitation energy were also identified. These states are depopulated by γ-ray transitions that bypass the long-lived 8^+ isomer. We have found two new transitions above the previously known (5^-) state at 2649 keV. This leads to the placement of the 3627 and 4226 keV states, with the tentative J^π assignments 7^- and 9^-, respectively. Such assignments are also supported by the $N = 50$ systematics (Fig. 5). We clearly see two new transitions, 257 and 976 keV, linking the 2649 keV state with the 2^+ state, via the 2391 keV state, which was previously tentatively identified

in the decay work of Ref. [20]. We confirm the existence of the 3723 keV state and we place a new state at 2806 keV with the tentative spin $J = 5$, which was deduced from the low R value of the 706 keV transition. A weak 381 keV γ-ray transition, linking the 2806 and 2424 keV states, is seen in a spectrum produced by a double gate on the 1415 and 684 keV transitions.

In the β-decay work of Ref. [20], spin and parity limits (4^+-8^+) and $(2^+, 4^+)$ were established for the 3723 and 2391 keV states, respectively. The fact that these states now also have been observed in a heavy-ion induced fusion-evaporation reaction suggests the choice of the highest possible spins. In this part of the level scheme, a few other transitions presumably belonging to ^{96}Pd were also seen, namely 760, 806, and 893 keV, but we could not firmly place them in the level scheme.

IV. DISCUSSION AND SHELL MODEL CALCULATIONS

In order to interpret states of the ^{96}Pd nucleus four different shell model calculations were performed and the results are presented in Fig. 6. Calculations marked GF were performed in the standard $(p_{1/2}, g_{9/2})$ proton (π) space, assuming a $^{88}_{38}$Sr$_{50}$ core, with the empirical interactions of Ref. [38]. This basic
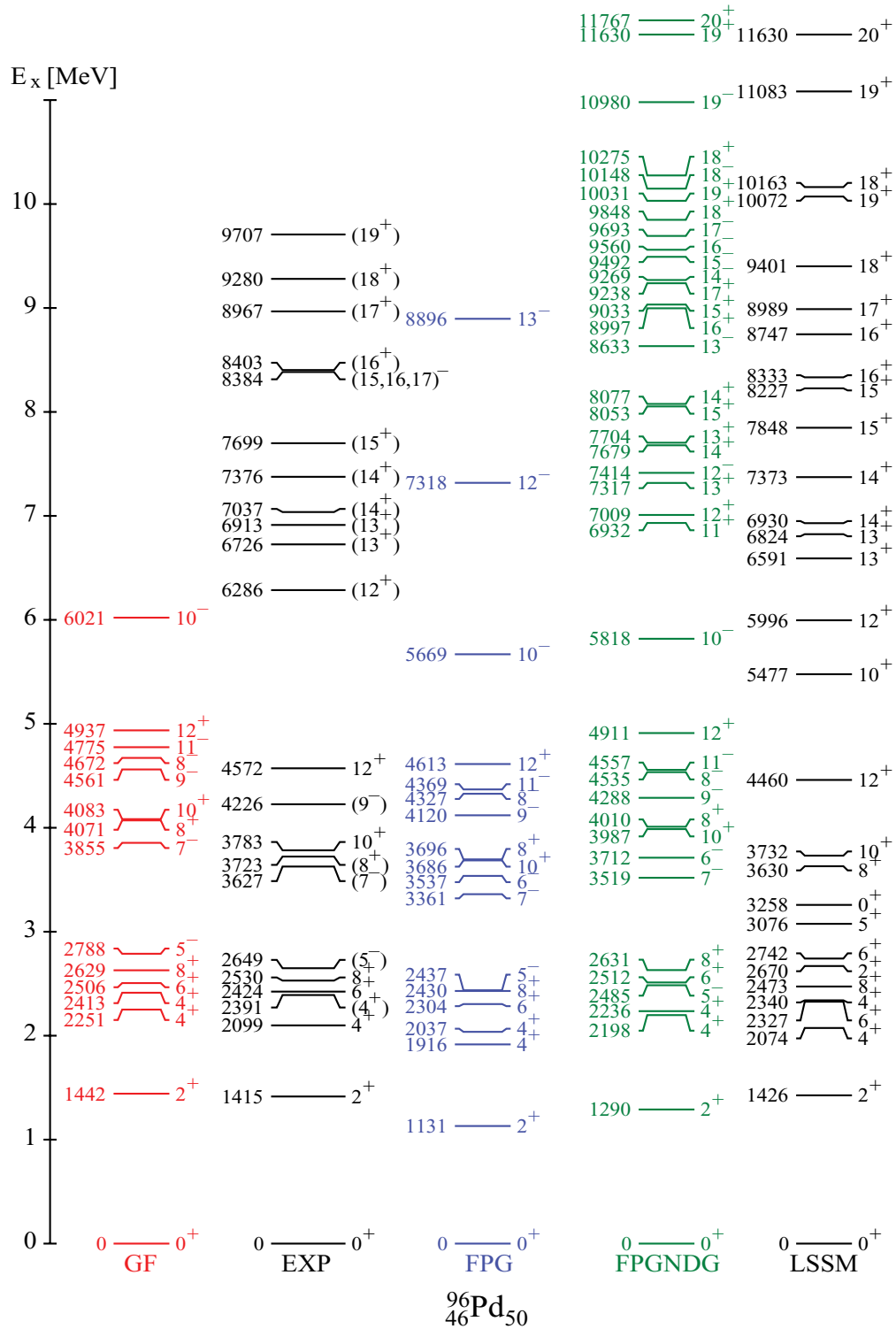
FIG. 6. (Color online) Experimental and shell model states for ^{96}Pd. See text for description of the shell model calculations.

model space reproduces the experiment remarkably well, up to the maximum spin state 12^+, although higher seniority states (above 8_1^+ and 5^-) are systematically calculated too high. This deficiency is partly cured in the calculations marked as FPG, were the GF model space was extended by including $\pi(f_{5/2}, p_{3/2})$ orbitals, with realistic interactions derived from

the charge-dependent Bonn (CD-Bonn) nucleon-nucleon potential [9,10]. The low-spin states in the FPG calculations are shifted too much down, though, which indicates that the pairing contribution should be tuned. This is due to the fact that the GF interaction was empirically fitted to the restricted model space which results in a "double counting" of the interaction
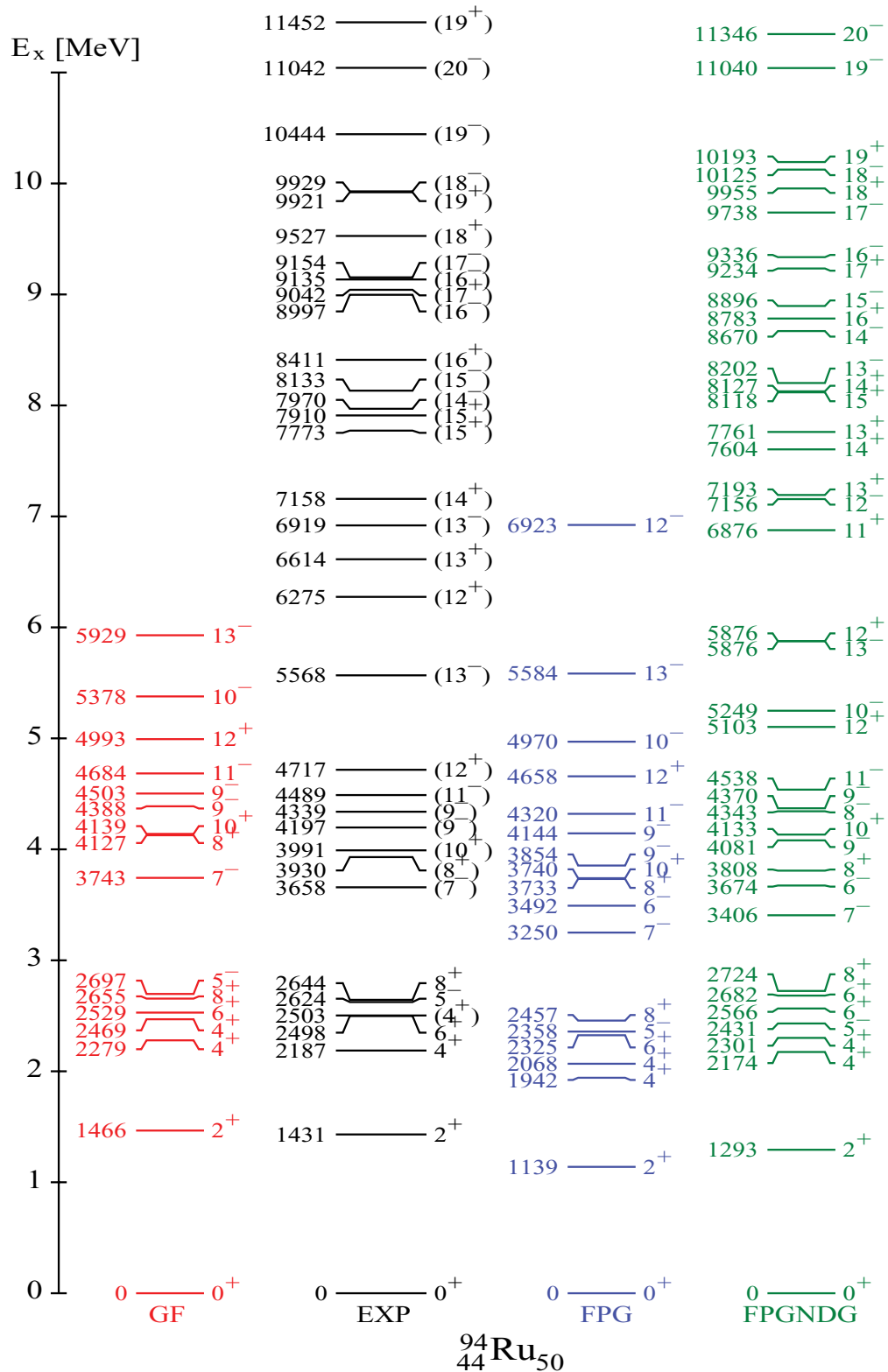
FIG. 7. (Color online) Experimental [12] and shell model states for ^{94}Ru (see text for details).

strength in the extended model space. For diagonal two-body matrix elements (TBME) this is most severe for the $T = 1$ pairing.

Even-parity states with spins higher than $12\hbar$ require $N = Z = 50$ core excitations. These states are reproduced very well in the large-scale shell model (LSSM) calculations

performed with the ANTOINE code [39,40], in which a $^{80}_{40}\text{Zr}_{40}$ core was assumed and up to five particle-hole excitations were allowed for $g_{9/2}$ protons and neutrons across the $N = Z = 50$ gap to the $g_{7/2}$, $d_{5/2}$, $d_{3/2}$, and $s_{1/2}$ orbitals. Note that no odd-parity orbitals are included in these calculations. The dominating components of all the wave functions of states above 12^+ and up to 19^+ include one-neutron excitations across the $N = 50$ to the $d_{5/2}$ orbital. The 19^+ state has the maximum possible spin in the $\pi g_{9/2}^{-4} \nu g_{9/2}^{-1} \nu d_{5/2}$ configuration. The 20^+ state can be reached with one-neutron particle-hole excitation to the $g_{7/2}$ orbital, and, for higher spin states, more than one excitation across the magic gap is needed. The LSSM calculations do not predict nanosecond or longer half-lives for any of its core-excited states.

Calculations marked as FPGNDG in Fig. 6 were done by implementing the FPG model space by single $g_{9/2}$ neutron particle-hole core excitations to the $d_{5/2}$, $g_{7/2}$ orbitals. The TBME for this extension of the model space were taken from the H7B interaction for $A = 100$ [41]. This interaction is based on a G matrix derived from the Paris potential [42]. This improves the agreement with the experiment for valence states, compared to FPG. Core-excited even-parity states are, however, predicted too high by about 560 keV on average compared to experiment and 500 keV higher than in the LSSM calculations. There seems to be a pronounced staggering, yielding larger differences for natural-parity states than for unnatural ones.

The FPGNDG model space is certainly too much truncated for the core-excited states. To get and idea about the odd-parity states in ^{96}Pd and about possible differences between the calculations and the experiment, we performed GF, FPG, and FPGNDG calculations for the ^{94}Ru nucleus, for which more rich experimental information exists. The results of these calculations are presented in Fig. 7. The valence states of ^{94}Ru up to 8^+ are again rather well described in all approaches. As in the case of ^{96}Pd, energies of higher seniority states are overestimated in the GF space, and the low lying FPG states are calculated about 200 keV too low. Inclusion of the core excitation in the model space (FPGNDG) improves the agreement. Higher up, the FPGNDG energies become too large. In ^{94}Ru the even- and odd-parity core-excited states are overestimated by about 270 and 580 keV on average, respectively (counting states from 13^+ to 19^+ and from 13^- to 20^-). This may indicate a tendency for a larger discrepancy in ^{96}Pd than in ^{94}Ru and also larger for the odd parity than for the even parity. Thus, a 1 MeV difference between the FPGNDG odd-parity states in ^{96}Pd and the real energies seems possible. Such a shift

TABLE III. Shell model (FPGNDG space) g factors for selected states in ^{96}Pd. Two different sets of assumptions on bare g factors were used in the calculations and are marked with (c) and (d)—see text for the values.

Spin and parity of the isomer	g factor value	
18^-	0.608 (c)	0.684 (d)
17^-	0.656 (c)	0.737 (d)
16^-	0.698 (c)	0.769 (d)
15^-	0.658 (c)	0.737 (d)
13^-	1.100 (c)	1.238 (d)
11^-	1.176 (c)	1.324 (d)
17^+	0.628 (c)	0.698 (d)

would bring the triple of $(15, 16, 17)^-$ shell model states in ^{96}Pd close to the experimental state at 8384 keV. The trend of staggering between odd and even spins is not reproduced in the calculations. The observed staggering effect may lead to shifting of the 16^- state below the 15^- state. The deviations between the FPGNDG model and the experiment are likely due to both the truncation and the inadequacy of the interaction.

The FPGNDG shell model transition strengths and g factors were calculated for different spin assignments of the isomeric state, and for the corresponding primary isomer decay transitions. The experimentally most likely $E1$ decays could not be calculated because $E1$ transitions are forbidden in this model space. Two different sets of effective charges were used for electric transitions which were found to be reasonable in such calculations [9,10]: (a) $e_\pi = 1.5e$, $e_\nu = 0.5e$; (b) $e_\pi = 1.72e$, $e_\nu = 1.44e$. Also, two different sets of the bare spin and angular-momentum g-factor values were assumed: (c) $g_s = 0.7g_s^{\text{free}}$, $g_s^\pi = 3.910$, $g_s^\nu = -2.678$, $g_l^\pi = 1$, $g_l^\nu = 0$; and (d) $g_s\pi = 3.896$, $g_s\nu = -2.136$, $g_l\pi = 1.16$, $g_l^\nu = -0.13$ [43]. The results of the calculations are listed in Tables II and III.

The $M2$ strength is low because an $M2$ transition in the adopted model space can result only from the $g_{9/2} \rightarrow f_{5/2}$ transition and the $f_{5/2}$ orbital is deep in the shell so its content in the wave functions is marginal. If the 685 keV transition were of type $M2$, the experimental reduced transition strength would be almost four orders of magnitude larger than the shell model value. A similar discrepancy is seen for an $E3$ decay. For an $E2$ decay, the experimental value is at least a few times larger than in the shell model, and energies of the unobserved transition lower than 100 keV would lead to significantly larger $E2$ experimental transition strengths. These discrepancies confirm the $E1$ scenario for the primary isomeric transition.

TABLE II. Shell model (FPGNDG space) and experimental transition strengths assuming different spin-parity and decay scenarios for the isomeric state in ^{96}Pd. Different sets of assumptions on effective charges and bare g factors were used and are marked with (a), (b), (c), and (d)—see text for the values. $E1$ decays are not calculated as they are forbidden in the adopted model space. The maximum transition energy of 100 keV was assumed to calculate the limit for an unobserved $E2$ decay.

Primary transition	σL	SM (W.u)		Experiment (W.u.)
$17^- \rightarrow 15^+$	$M2$	3.87×10^{-5} (c)	4.16×10^{-5} (d)	0.26
	$E3$	4.34×10^{-2} (a)	5.70×10^{-2} (b)	8.4×10^2
$17^- \rightarrow 15^-$	$E2$	4.23 (a)	8.25 (b)	>24

The measured g-factor value [23] slightly favors the 16^- assignment (see Table III). One should, however, keep in mind that g factors for all core-excited states, of even or odd parity, are very similar and therefore not really selective.

It is worth mentioning that the comparison of yrast spectra of the $N = 50$ isotones (Fig. 5) shows a lack of the 11^- and 13^- states in ^{96}Pd, which both should lie below the isomer. Inspection of the FPGNDG wave functions and $E2$ strengths gives a natural explanation for the nonobservation of these states. The $15^- \rightarrow 13^-$ transition is blocked as the 13^- state is mainly FPG while the 15^- state (as 14^-, 16^-, 17^-) is FPGNDG. This difference is reflected in the g-factor values of these states (see Table III). This is why a possible $(15, 16, 17)^-$ isomer chooses the $E1$ path. Note also that the yrast 13^- state in ^{94}Ru is a pure $p_{1/2}^{-1} g_{9/2}^{-5}$ state which is not possible for the four-hole nucleus ^{96}Pd.

V. CONCLUSIONS

The level scheme of ^{96}Pd was extended up to an excitation energy of 9707 keV and a tentative spin and parity of 19^+. Low-lying negativeparity yrast states were also identified, up to 4226 keV, with the tentative assignment $J^\pi = 9^-$. States above an excitation energy of 4572 keV are interpreted as $N = 50$ core excitations. An isomeric state with a half-life of 37.7(1.1) ns was identified at an excitation energy of 8384 keV.

Negative parity and a spin value in the range $15\hbar$ to $17\hbar$ was tentatively assigned to this state, giving experimental evidence of interactions of the $N = 50$ core-excited neutrons with the negative-parity proton holes of the fpg shell. Shell model calculations in the full fpg shell with just one particle-hole excitation across the magic $N = Z = 50$ gap provide a qualitative description of the isomer. A more complete and consistent model is, however, needed to quantitatively reproduce the isomer and its decay, with larger model space, improved interactions in the negative-parity orbitals, and more core particle-hole excitations allowed. In addition, further experimental work is required to make firm spin and parity assignments of the isomeric as well as of the other observed states in ^{96}Pd.

[1] A. Poves and G. Martinez-Pinedo, Phys. Lett. B **430**, 203 (1998).

[2] W. Satuła, Phys. Scr., T **125**, 82 (2006).

[3] E. Caurier, F. Nowacki, A. Poves, and K. Sieja, Phys. Rev. C **82**, 064304 (2010).

[4] D. Seweryniak *et al.*, Phys. Rev. Lett. **99**, 022504 (2007).

[5] I. Darby *et al.*, Phys. Rev. Lett. **105**, 162502 (2010).

[6] B. Cederwall *et al.*, Nature (London) **469**, 68 (2011).

[7] B. S. Nara Singh *et al.*, Phys. Rev. Lett. **107**, 172502 (2011).

[8] H. Schatz *et al.*, Phys. Rev. Lett. **86**, 3471 (2001).

[9] T. Brock *et al.*, Phys. Rev. C **82**, 061309(R) (2010).

[10] P. Boutachkov *et al.*, Phys. Rev. C **84**, 044311 (2011).

[11] K. Muto, T. Shimano, and H. Horie Phys. Lett. B **135**, 349 (1984).

[12] H. A. Roth *et al.*, Phys. Rev. C **50**, 1330 (1994).

[13] M. Lipoglavšek *et al.*, Phys. Rev. C **66**, R011302 (2002).

[14] M. Lipoglavšek *et al.*, Phys. Rev. C **65**, R051307 (2002).

[15] D. Sohler *et al.*, Nucl. Phys. A **708**, 181 (2002).

[16] A. Blazhev *et al.*, Phys. Rev. C **69**, 064304 (2004).

[17] A. Blazhev *et al.*, J. Phys.: Conf. Ser. **205**, 012035 (2010).

[18] M. Lipoglavšek, M. Vencelj, C. Baktash, P. Fallon, P. A. Hausladen, A. Likar, and C. H. Yu, Phys. Rev. C **72**, 061304(R) (2005).

[19] W. Kurcewicz *et al.*, Z. Phys. A **308**, 21 (1982).

[20] L. Batist *et al.*, Nucl. Phys. A **720**, 245 (2003).

[21] H. Grawe and H. Haas, Phys. Lett. B **120**, 63 (1983).

[22] W. F. Piel Jr., G. Scharff-Goldhaber, C. J. Lister, and B. J. Varley, Phys. Rev. C **28**, 209 (1983).

[23] D. Alber, H. H. Bertschat, H. Grawe, H. Haas, and B. Spellmeyer Z. Phys. A **332**, 129 (1989).

[24] A. B. Garnsworthy, Phys. Rev. C **80**, 064303 (2009).

[25] J. Simpson *et al.*, Z. Phys. A **358**, 139 (1997).

[26] W. Korten and S. Lunardi (eds.), EUROBALL Scientific and Technical Activity Report 1997–2003, 2003 (unpublished), [http://www-dapnia.cea.fr/Sphn/Deformes/EB/eb-report-final. pdf].

[27] G. Duchêne *et al.*, Nucl. Instrum. Methods A **423**, 90 (1999).

[28] J. Eberth *et al.*, Nucl. Instrum. Methods A **369**, 135 (1996).

[29] Ö. Skeppstedt *et al.*, Nucl. Instrum. Methods A **421**, 531 (1999).

[30] J. Ljungvall, M. Palacz, and J. Nyberg, Nucl. Instrum. Methods A **528**, 741 (2004).

[31] M. Palacz *et al.*, Nucl. Instrum. Methods **550**, 414 (2005).

[32] M. Palacz, J. Cederkäll, M. Lipoglavšek, L.-O. Norlin, J. Nyberg, and J. Persson, Nucl. Instrum. Methods A **383**, 473 (1996).

[33] D. C. Radford, Nucl. Instrum. Methods A **361**, 290 (1995).

[34] R. Brun and F. Rademakers, Nucl. Instrum. Methods A **389**, 81 (1997).

[35] H.-Q. Jin (unpublished).

[36] N. G. Nicolis, D. G. Sarantites, and J. R. Beene, Computer code EVAPOR (unpublished), see also [ftp://ftp.phy.ornl.gov/pub/ evapOR/].

[37] N. S. Pattabiraman *et al.*, Phys. Rev. C **65**, 044324 (2002).

[38] R. Gross and A. Frenkel, Nucl. Phys. A **267**, 85 (1976).

[39] E. Caurier and F. Nowacki, Acta Phys. Pol. B **30**, 705 (1999).

[40] E. Caurier, G. Martínez-Pinedo, F. Nowacki, A. Poves, A. P. Zuker *et al.*, Rev. Mod. Phys. **77**, 427 (2005).

[41] A. Hosaka, K.-I. Kubo, and H. Toki, Nucl. Phys. A **444**, 76 (1985).

[42] M. Anantaranam, H. Toki, and G. F. Bertsch, Nucl. Phys. A **398**, 269 (1983).

[43] H. Grawe *et al.*, Hyperfine Interact. **15**, 65 (1983).